A parametric study on pulse duplicator design and valve hemodynamics

Received: 30 October 2023 | Revised: 1 February 2024 | Accepted: 4 April 2024

DOI: 10.1111/aor.14757

Artificial Organs WILEY

MAIN TEXT

A parametric study on pulse duplicator design and valve hemodynamics

Caroline C. Smid[1] | **Georgios A. Pappas**[1] | **Volkmar Falk**[2,3,4] | **Paolo Ermanni**[1] | **Nikola Cesarovic**[2,3]

[1]Laboratory of Composite Materials and Adaptive Structures, ETH Zurich, Zürich, Switzerland

[2]Translational Cardiovascular Technologies, ETH Zurich, Zürich, Switzerland

[3]Department for Cardiothoracic and Vascular Surgery, Deutsches Herzzentrum der Charité, Charité Universitätsmedizin Berlin, Berlin, Germany

[4]German Center for Cardiovascular Research (DZHK), Partner Site Berlin, Berlin, Germany

Correspondence
Caroline C. Smid, Laboratory of Composite Materials and Adaptive Structures, ETH Zurich, Leonhardstrasse 21, 8092 Zürich, Switzerland.
Email: csmid@ethz.ch

Funding information
Zurich Heart, Hochschulmedizin Zürich, Switzerland; ETH Zürich, Switzerland; ETHeart, Open ETH, ETH Board, Switzerland

Abstract

Background: In vitro assessment is mandatory for artificial heart valve development. This study aims to investigate the effects of pulse duplicator features on valve responsiveness, conduct a sensitivity analysis across valve prosthesis types, and contribute on the development of versatile pulse duplicator systems able to perform reliable prosthetic aortic valve assessment under physiologic hemodynamic conditions.

Methods: A reference pulse duplicator was established based on literature. Further optimization process led to new designs that underwent a parametric study, also involving different aortic valve prostheses. These designs were evaluated on criteria such as mean pressure differential and pulse pressure (assessed from high-fidelity pressure measurements), valve opening and closing behavior, flow, and regurgitation. Finally, the resulting optimized setup was tested under five different hemodynamic settings simulating a range of physiologic and pathologic conditions.

Results: The results show that both, pulse duplicator design and valve type significantly influence aortic and ventricular pressure, flow, and valve kinematic response. The optimal design comprised key features such as a compliance chamber and restrictor for diastolic pressure maintenance and narrow pulse pressure. Additionally, an atrial reservoir was included to prevent atrial–aortic interference, and a bioprosthetic valve was used in mitral position to avoid delayed valve closing effects.

Conclusion: This study showed that individual pulse duplicator features can have a significant effect on valve's responsiveness. The optimized versatile pulse duplicator replicated physiologic and pathologic aortic valve hemodynamic conditions, serving as a reliable characterization tool for assessing and optimizing aortic valve performance.

KEYWORDS

aortic valve, bioprosthetic valve, hemodynamic settings, mechanical valve, polymeric valve, pulse duplicator, valve characterization

1 | INTRODUCTION

Despite the continuous and considerable improvement of prosthetic heart valves, there is no certified heart valve prosthesis that fulfills both hemodynamic and durability requirements, without the need for anticoagulation.[1] This underscores the imperative for continuous development toward novel heart valve designs and concepts, driven by the annual demand for over 300 000 prosthetic heart valves globally.[2–4] Pulse duplicators (PD) are employed for in vitro valve testing, aiming at both device development and long-term durability assessment, under various physiologic and pathologic hemodynamic conditions. This reduces the need for in vivo animal studies, where apart from the obvious ethical concern, certain hemodynamic settings cannot be studied.[5,6]

However, only a few specific PD platforms are recognized by regulatory bodies worldwide and commercialized, such as ViVitro Labs (Victoria, Canada), Dynatek Labs (Galena, MO, USA), and BDC Labs (Wheat Ridge, CO, USA), while other concepts may be used for research purposes, with the basic principle to remain the same. In most cases, only the left heart domain is emulated. The cardiac cycle is induced by piston-driven pumps or with indirect mechanisms, including similar pumps or pneumatic actuators,[7–16] aiming to generate a pulsatile flow with adjustable cardiac output (CO).

The majority of PDs include an aortic valve (AV) and mitral one (MV) with two chambers that simulate the left ventricle and atrium, additionally featuring anatomical compliance and peripheral resistance. PD valve assessment often employs pressure and flow sensors, as well as optical techniques. While water is commonly employed as the circulating fluid, a water–glycerin mixture (e.g., 40/60% w/w[17]) is often utilized to approximate better blood's viscosity. Despite basic similarities in design principles of PDs, differences arise in certain characteristics as ISO5840-3[18] provides conceptual guidelines but lacks explicit design specification. It specifies detailed requirements for the measuring equipment accuracy, but equivalent specificity is absent for PD features potentially crucial for physiologic valve performance. This is also depicted in the round-robin study, where commercial PD and systems from top institutions are compared, and results show significant variation.[19] Establishing standard parameters such as heartbeat rate or CO in a PD environment can be straightforward, but a physiologic pressure condition and flow environment cannot be trivially achieved.[6] Thus, proper calibration of a PD is crucial. Moreover, the interaction between PD design and imposed conditions, especially on pressure history (pressure profile over heartbeat time), has not been thoroughly investigated, despite the fact that proper valve exposure to physiologic pressure environment is crucial.

The objective of this study is to investigate the effects of PD features on valve responsiveness and conduct a sensitivity analysis across valve prosthesis types. This analysis contributes to the development of versatile PD systems able to perform reliable prosthetic aortic valve assessment under physiologic hemodynamic conditions. Starting from a literature-based PD, alternative designs were developed and tested using three different valve prosthesis types (bioprosthetic, mechanical, polymeric). The parametric study identified an optimized PD design and investigated the influence of mechanical features that emulate aspects such as compliance and resistance. The evaluation is based on comparison of pressure and flow history with the physiologic equivalent. For completeness, various hemodynamic conditions (e.g., hypertension, tachycardia, etc.) were also imposed on the optimized PD design, assessing the reliability of replicating a range of physiologic and pathologic hemodynamic conditions.

2 | MATERIALS AND METHODS

2.1 | Reference PD design

Based on a literature review,[12,20-23] a reference PD (denoted as 'ref.') was designed and realized, emulating the left heart domain PD, as shown in Figure 1A. In the PD, the fluid is pulled through the MV by a pulsatile piston pump (ViVitro Labs Inc., Victoria, Canada, Cylinder Area: 38.32 cm^2), with maximum stroke volume (SV) of ~300 mL, mimicking the left ventricle. The MV experiences an atrial pressure of approximately 5 mmHg[26] imposed by an elevation-induced hydrostatic pressure, by means of a 3 L reservoir filled with ~1.8 L (×20 SV of 70 mL; see section 2.4) that mimics the left atrium. The systole is emulated by the liquid being pushed from the piston pump through the AV via the outlet. The AV is positioned in a compliant elastomeric 3D-printed (Elastic 50A Resin, Formlabs, MA, USA) aortic root model based on design parameters found in Swanson and Clark,[27] with an additional outlet to air bleed the setup, which is used for the MV too. Post-aortic systemic compliance and resistance are crucial. In the PD, flow is directed from the aortic root to a compliance chamber (~0.5 L) filled with water and pressurized air, mimicking systemic compliance contributing to a smooth flow. From the compliance chamber, water flows into a second, column-shaped reservoir (~4.8 L), imposing aortic resistance. This design concept aims to increase aortic resistance while simultaneously providing a continuous hydrostatic pressure on the AV, similar to literature [12,20-23]. This setup mimics

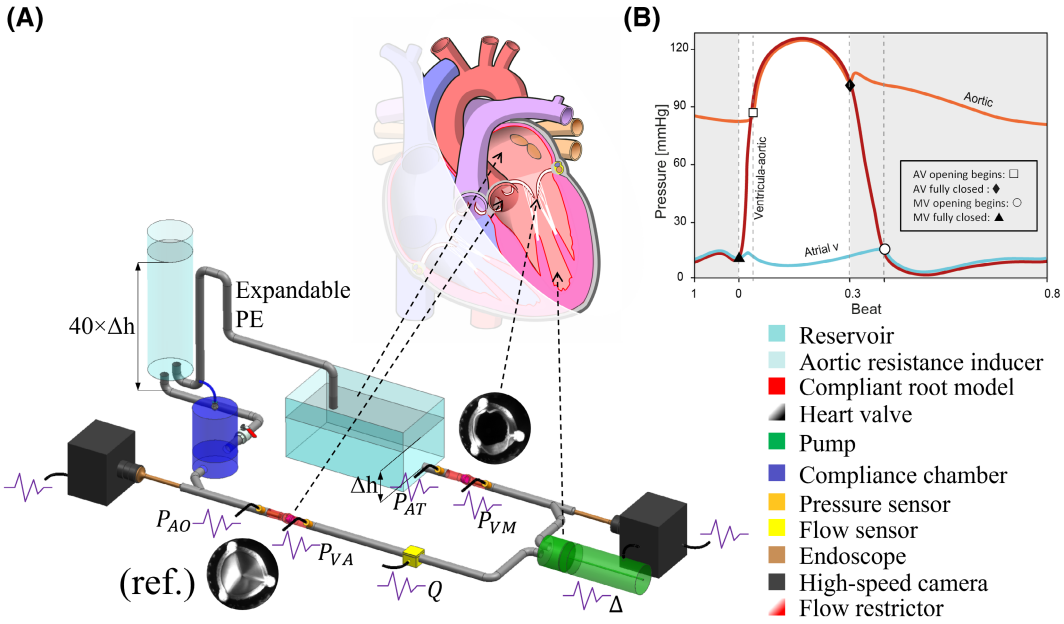

FIGURE 1 (A) Schematic drawing (not to scale) of reference PD setup (denoted 'ref.') with its anatomical equivalent shown with a heart model from Jahren et al. [24]; (B) idealized aortic and ventricular pressure curve based on information from Miller-Hance and Gertler [25].

the anatomical conditions at a standing position and helps maintain diastolic aortic pressure. Via a syphon system, used to maintain the water level in the column, the water flows back into the atrial reservoir closing the circuit. The tubes that allow the flow are rigid, transparent polyvinyl chloride (PVC) ones with an inner diameter of 19 mm and 3 mm thickness, except for an extendable polyethylene (PE) drain hose as the syphon connecting the water column and atrium. The circulating medium is distilled water at room temperature (21 ± 2°C).

2.2 | Instrumentation, data acquisition, and analysis

The evaluation of valve behavior involves flow measurements, high-fidelity pressure data, and real-time imaging. These data are acquired and subsequently analyzed using a MATLAB script developed in-house. The output voltage of all devices is recorded by a microcontroller board equipped with a 12-bit analog-to-digital converter, ADC (Arduino Due). The flow is imposed by the pulsatile pump in a sinusoidal form with adjustable amplitude and wavelength/frequency and systole over diastole ratio of 1/2. The piston position ($\Delta(t)$) is used to calculate the imposed volume rate ($\dot{V}$), heartbeat, and define the start and end of systole. The aortic flow rate (Q_{AV}) is measured with a flow sensor (SONOTEC GmbH, Halle (Saale), Germany) with an accuracy of ±100 mL/min (in the range of 0–5 L/min) upstream of the AV and is later correlated with $\Delta(t)$. The actual CO (L/min), as well as the regurgitation (V_R), is determined based on averaged (10 cycles) instant flow rate (Q_{AV}) data (Figure 4).

Two pressure sensors (Sensata Technologies, MA, USA), positioned about 80 mm upstream and downstream of the AV, capture ventricular-aortic (P_{VA}) and aortic (P_{AO}) pressure, respectively, as well as atrial (P_{AT}) and ventricular-mitral (P_{VM}) pressure for the MV. The pressure sensors being lateral to the flow measure only hydrostatic pressure, within the range of 0–500 mbar (0–375 mmHg) with a fidelity (linearity and hysteresis) of at least 0.025% of the full range, which coincides with the resolution of the ADC system (0.9 mmHg). The reference pressure is taken by the surrounding atmospheric environment. The pressure differential ($\Delta P(t)$) for the AV is evaluated over a full cycle and calculated as

$$\Delta P(t) = P_{VA}(t) - P_{AO}(t) \quad (1)$$

The mean pressure differential $\Delta\overline{P}$, often referred to as mean pressure gradient,[18] is the averaged $\Delta P(t)$ per cycle, keeping only positive values.[18]

To assess valves' responsiveness, two laparoscopic endoscopes (Hopkins II, Karl Storz, Tuttlingen, Germany) are inserted into 45°-Y-fittings, laying coaxially to the AV and MV. The valve's motion is recorded from the downstream side with a high-speed camera (FASTCAM Mini UX100, Photron USA Inc. and MeVis-C 1.6/35 macro lens, LINOS, Göttingen, Germany) at a frame rate of 250 fps and a resolution of 1280 × 1024pix^2, positioned to the eyepiece of each endoscope. Two continuous light sources arranged around the heart valves are used for

illumination. After triggering the camera, a signal is sent, for every captured image, to the microcontroller board (with a fidelity of 125 µs) to allow synchronous data acquisition. Concurrently, pressure, flow, and position data points are recorded with a sampling rate of 3 kHz, enabling the capture of fast events, such as valve opening that occurs in a ms range. Characteristic points such as start of opening and closing, fully opened and closed state, are determined based on the taken images. During post-processing, the final values are averaged over ten consecutive cycles, along with standard deviation.

2.3 | Parametric study on PD designs

The literature demonstrates various PD design approaches; however, there is limited understanding regarding the distinct effects of these variations in order to determine a superior design. Therefore, more PD designs were developed herein by not only changing the resistance, enhancing compliance, but also addressing secondary features.

The column-shaped reservoir was removed, the aortic side was elevated, and a restrictor was added after the compliance chamber for variations ((i)–(vi)) depicted in Figure 2. The restrictor, models peripheral resistance, replacing the hydrostatic column, and can be adjusted for desired peak systolic pressure. These variations still comply with ISO5840-3[18] as there are very few specific design requirements,[19] while compliance chambers are optional.

The evaluation of the PD designs is based on the following criteria: (a) $\Delta P(t)$; (b) $\Delta \overline{P}$; (c) pulse pressure (PP); (d) valve opening and closing behavior; (e) Q_{AV}; and (f) V_R. The PP is determined using the following formula:

$$PP = P_{Systolic} - P_{Diastolic} \tag{2}$$

Here, $P_{Systolic}$ represents peak P_{AO}, and $P_{Diastolic}$ corresponds to the minimum P_{AO}.

The three investigated AVs have a 22 ± 1 mm nominal inner diameter (ID), namely (1) bioprosthetic heart valve (BHV) (Edwards INTUITY Elite 21 mm), (2) mechanical (MHV) (Medtronic Advantage outer diameter: 27 mm and ID: 23 mm), and (3) polymeric (polyurethane, PU-CARBOTHANE™ PC-3585A) (PHV) with a 22 mm ID following the design by Leat and Fisher [28,29]. The latter was prepared in-house, with PU leaflets dip-coated by means of an aluminum mold, over a 3D-printed stent (Therma 289, DWS). For the mitral position, the aforementioned BHV model was used. The three AVs are assessed for each alteration under normotensive hemodynamic setting ① (see section 2.4). Due to system complexity, the focus was on isolation of dominant parameters to understand individual effects. Given the scale of potential combinations, a full exploration of all parameters was beyond the scope of this study and can be the content of future studies.

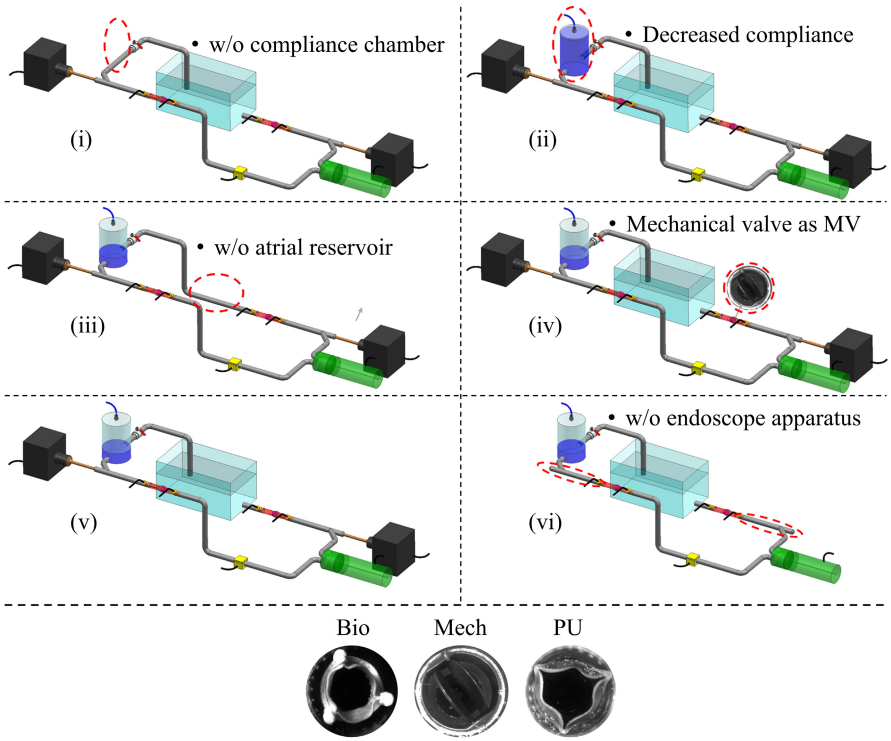

FIGURE 2 Top: Schematic (not to scale) of investigated PD configurations (i)–(vi), to be compared with (ref.) (Figure 1), note the absence of the column reservoir, elevation of aortic side, and addition of a restrictor, while other modified areas are circled in red. Bottom: The three different valve prostheses attested imaged during testing at an open state.

2.4 | Hemodynamic settings

PDs are meant to assess pressure and flow history of various valve types under physiologic and pathologic conditions. To evaluate hemodynamic versatility of the optimized PD, a BHV was attested in aortic position based on the aforementioned criteria (see section 2.3), for five hemodynamic settings listed in Table 1 following ISO 5840-3.[18] The restrictor setting, as well as pump frequency and amplitude, was adjusted to achieve these hemodynamic settings. The nominal CO was referenced by the value identified by the flow sensor for (ref.) with the BHV, to serve as benchmark to identify $\Delta(t)$, which was maintained for all variations (per hemodynamic setting). For this benchmark, a nominal of 5 L/min correlates to an imposed $\dot{V}$ of ~6.3 L/min. As explained in section 3.1.4, the actual CO is always lower (10%–90%) than $\dot{V}$, as fluid is also flowing through the mitral outlet. This discrepancy depends on valve type and PD design.

3 | RESULTS AND DISCUSSION

In summary, the parametric study demonstrated strong influence of various features on pressure and flow history. The subsequent analysis identified alteration (v) (Figure 3), as the most optimal configuration, reliably replicating natural physiologic conditions, having a compliance chamber and flow restrictor. The results of this configuration are used as a baseline for comparison.

3.1 | PD response as a function of design and valve

The pressure and flow history with hemodynamic setting ① on (v) can be seen in Figure 4A–C. The aortic pressure curves closely resemble the physiologic equivalent (Figure 1B), achieving a hemodynamic condition akin to 120/80 mmHg with a PP of ~50 mmHg. In systole, P_{VA} exhibits a slight elevation compared to P_{AO}, both following a similar waveform. Furthermore, P_{AO} decreases toward the end of systole, creating a distinct peak as the AV closes. In diastole, P_{AO} steadily declines, whereas P_{VA} experiences a sudden drop (see Figures 1B and 4A–C) that may even reach negative values, out of the sensing range, attributed to the piston actuation (see section 3.2). The flow curve exhibits a physiologic pattern, characterized by a sharp rise and a gradual decline. Images of the bioprosthetic AV and MV in (v) at characteristic points are displayed in Figure 4D, confirming AV's physiologic behavior, showing complete opening and closing synchronized with the cardiac cycle. Figure 5 shows that the MHV exhibits higher V_R due to late closing. This is evident in Figure 4A–C, where P_{VA} drops later (0.52 s for MHV vs. 0.49 s for BHV and PHV). Furthermore, the PHV has the highest $\Delta\overline{P}$ (on average 1 mmHg more than the BHV) as illustrated in Figure 5.

3.1.1 | Influence of column-shaped reservoir

With all valve prostheses using the column-shaped reservoir in (ref.), the actual CO remains consistent, $\Delta\overline{P}$ experiences either no change or a slight increase, and V_R decreases. On one hand, the pressures in Figure 6A–C illustrate accelerated ascension of aortic pressure due to a delayed AV opening. The delay is due to constant exposure of the AV to water column pressure, subsequently inducing a hydrostatic pressure (meant to be P_{AO}), which apparently leads to a delayed AV closing subsequent to a prolonged pressure decline. The consequence is an increased PP of about 100 mmHg (125/20 mmHg), accompanied by a gradual Q_{AV} reduction during the latter half of systole.

Furthermore, P_{VM} increases by 15–48 mmHg compared to (v) (or more as sensing limit is often reached), due to delayed ultimate opening of AV (in the range of 12–24 ms), causing a prolonged pressure build-up on the mitral side (see Figure 6A–C). Despite minimal flow disturbance, the reservoir-induced resistance fails to achieve a physiologic pressure history.

3.1.2 | Influence of compliance chamber

The created compliance chamber emulates aortic and systemic compliance, with a compressible air-filled cavity, adding dampening ability on the flow and inertia to the system. All these promote the transition of pulsatile to continuous flow, as well as the shortening and delaying of volume passing through the AV,[30] contributing to a delay and slower decrease in Q_{AV}, in its absence. Moreover, the reduced aortic resistance leads to a lower $\Delta\overline{P}$ and an elevated actual CO for a given $\dot{V}$. The overlapping of P_{AO} and P_{VA} (Figure 6D–F) suggests an elevated PP alongside a shortened duration of increased pressure. Throughout systole, P_{VM} decreases, displaying a faster initial increase followed by a gradual decline (Figure 6D–F). Reduced compliance, according to O'Rourke's and Hashimoto's[31] human model, leads to elevated systolic pressure due to reduced vessel distensibility and wave reflection. Notably, the plots lack a rise in systolic pressure since the aortic restrictor is adjusted to approximate a peak of ~120 mmHg. Rigid tubes allow for minimal wave dampening, causing earlier wave

Nominal pressure condition [mmHg]		Heart rate [bpm]	SV [mL]	Nominal CO [L/min]
①	Normotensive (120/80)	70	~70	5
②	Normotensive (120/80)	140	~35	5
③	Normotensive (120/80)	140	~70	10
④	Severe hypertensive (210/120)	70	~70	5
⑤	Severe hypertensive (210/120)	140	~70	10

TABLE 1 Hemodynamic settings for valve assessment. Note that actual CO corresponds to flow sensor-based measurement.

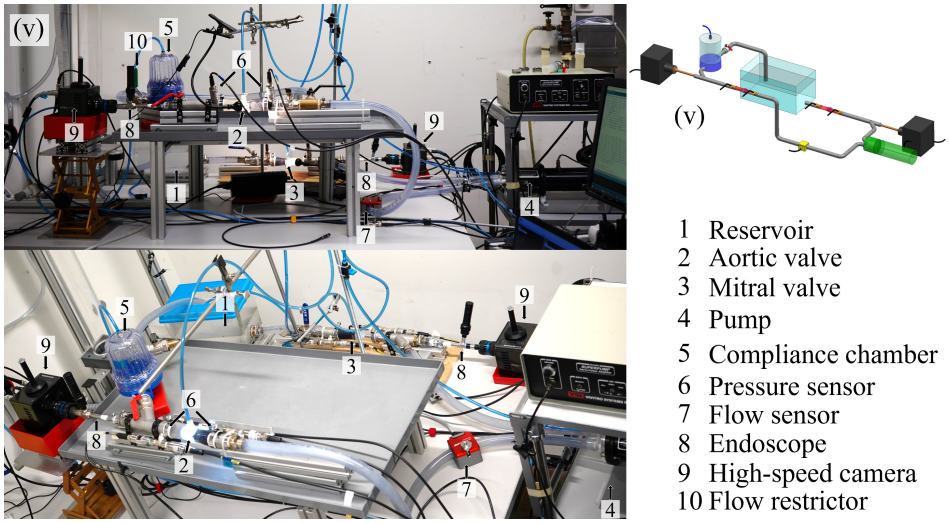

FIGURE 3 Pictures of the optimized PD (v) and schematic.

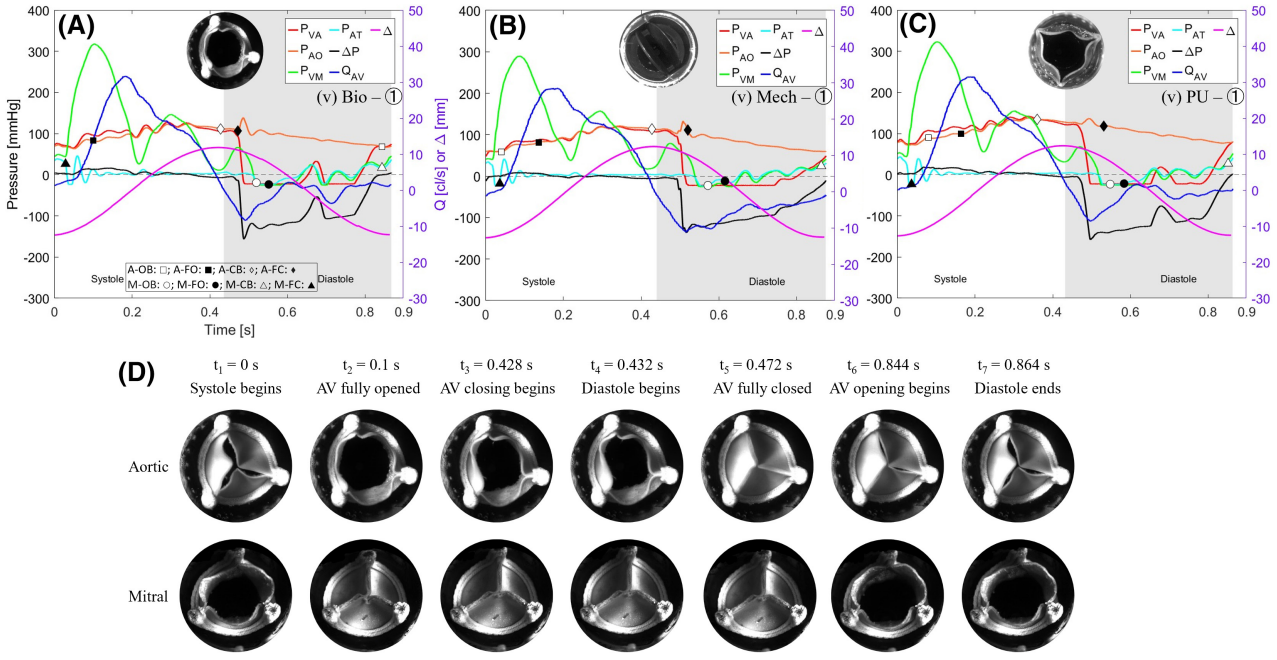

FIGURE 4 (A)–(C) Pressure and flow history (mean of 10 cycles) with (v) for a (A) BHV, (B) MHV, and (C) PHV in aortic position with hemodynamic setting ①. A: aortic; M: mitral; OB: opening begins; FO: fully opened; CB: closing begins; FC: fully closed. (D) Images with (v) for BHV in aortic and mitral position with hemodynamic setting ①.

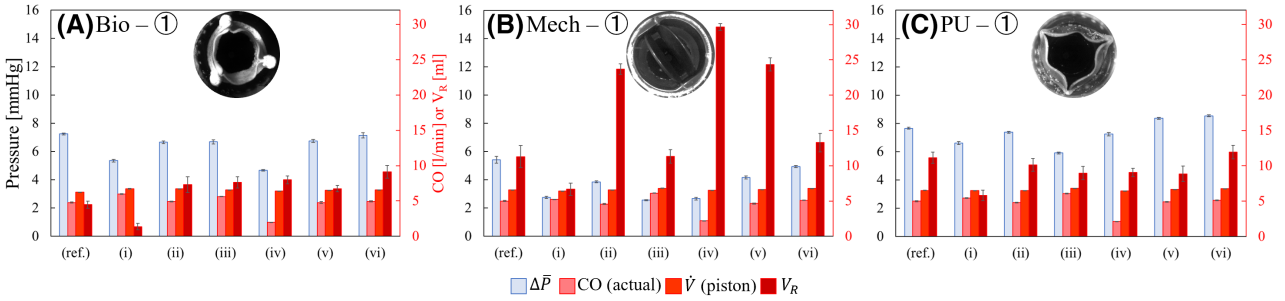

FIGURE 5 $\Delta\overline{P}$, CO (actual), $\dot{V}$ (piston), and V_R (mean of ten cycles) of (ref.) and all alterations (i)–(vi) for (A) BHV, (B) MHV, and (C) PHV in aortic position for hemodynamic setting ①.

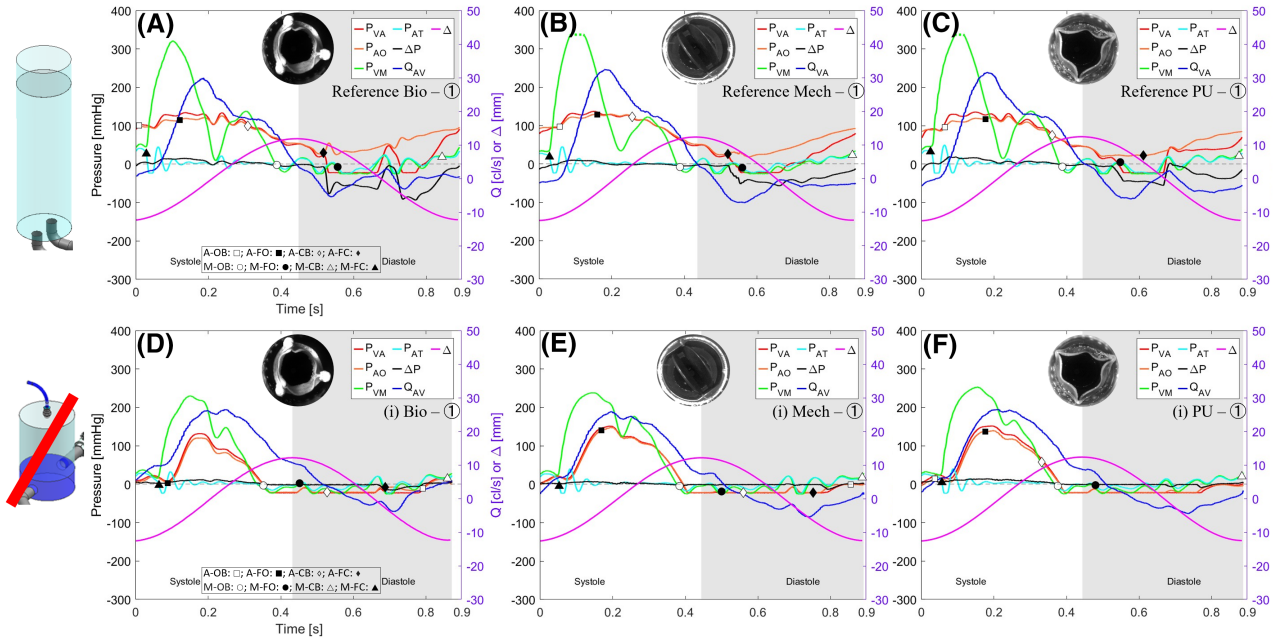

FIGURE 6 Pressure and flow history (mean of ten cycles) with (ref.) (A–C) and alteration (i) (D–F) for BHV, MHV, and PHV in aortic position with hemodynamic setting ①. A: aortic; M: mitral; OB: opening begins; FO: fully opened; CB: closing begins; FC: fully closed. Note that the dashed line indicates pressure beyond detection range.

reflection, elevating pressure in late systole instead of diastole, ultimately enhancing PP.[31] Early wave reflection potentially explains the challenge in sustaining P_{AO} over diastole given the absence of continuous pressure from water storage and pressurized air.

Decrease in compressed air within the chamber, to reduce compliance, yields comparable, yet less pronounced patterns than the total absence of the compliance chamber, as depicted in Figure 7A–C. The CO remains relatively consistent or slightly elevated, while the average $\Delta\overline{P}$ experiences a marginal reduction. Both PP and P_{VM} decrease, too. However, reduced compliance, as opposed to complete absence, leads to higher V_R. This rise can be attributed to the compliance chamber serving as a small water reservoir, ensuring greater water availability downstream to the AV during reverse flow. Compared to high compliance scenarios, a reduction or absence of compressible air cavity yields reduced water storage and more disrupted flow in the drainage tube.

3.1.3 | Influence of atrial reservoir

Without the atrial reservoir, both MV and AV (Figure 7D–F) are directly affected due to their series connection. Instead of water storage along with a dampening mechanism, the flow is immediately directed from the compliance chamber through the MV. Atrial systole effect is induced through the atrial reservoir utilizing imposed hydrostatic pressure. Despite regarded optional according to the ISO 5840,[18] this reservoir proves to be of high importance.

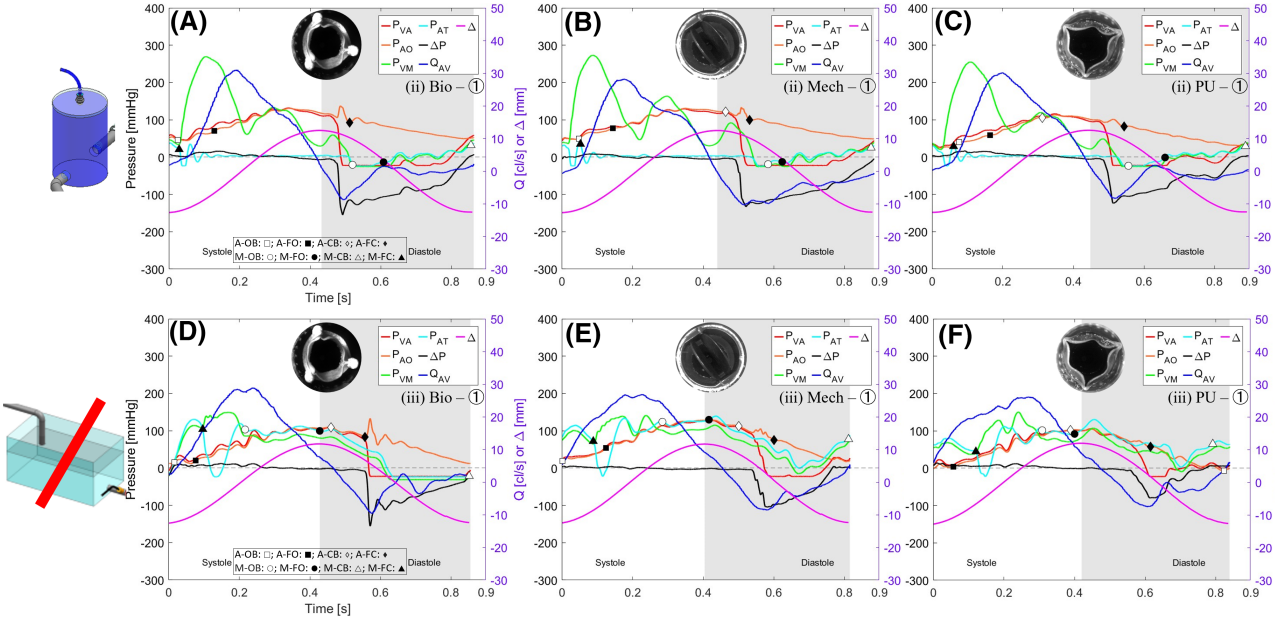

FIGURE 7 Pressure and flow history (mean of ten cycles) with alterations (ii) (A–C) and (iii) (D–F) for BHV, MHV, and PHV in aortic position with hemodynamic setting ①. A, aortic; CB, closing begins; FC, fully closed; FO, fully opened; M, mitral; OB, opening begins.

Consequently, during systole, pump's volume change retains the MV closed from the ventricular side, while simultaneously forcing it to open from the atrial side given that the AV has already opened. Additionally, the elevated hydrostatic pressure caused by the height difference forces the MV to open, all resulting in a shortened closed period with early mid-systolic opening.

Moreover, the AV remains open over an extended period and closes only during diastole leading to a significantly slower decrease of Q_{AV}. Piston's retraction is forcing the AV to close from the ventricular side, while simultaneously pushing it open from the aortic side through the open MV. This results in elevated CO and PP. Despite very similar behavior of the three different AVs, there is no discernible trend in V_R. Namely, the BHV shows a minor increase, the MHV a decrease, and the PHV no change. $\Delta\overline{P}$ is reduced for both MHV and PHV. The examination was limited to the two extremes: employing a large reservoir (×20 SV) and its complete absence. Nevertheless, the study showed that the provided inertia to the system is essential for physiologic behavior.

3.1.4 | Mitral valve type and secondary effects

A similar effect to the one of MHV on the aortic side (see Figure 5), was observed when MHV is in mitral position, showing delayed closing[17,32] resulting in higher V_R. Despite assumptions about larger diameter to contribute to this, no direct connection exists.[12] The delayed closing results in a notable reduction in actual CO on the aortic side, accompanied by a significant decrease in P_{VM} with less pronounced local peaks, as illustrated in Figure 8A–C. This phenomenon arises from the circumstance that, during the initial systolic phase, a greater volume can pass through the MV at a reduced resistance, bypassing the naturally closed AV. For instance, the PP of the BHV decreased from 61 mmHg (124/63 mmHg) to 29 mmHg (127/98 mmHg). The apparent lower $\Delta\overline{P}$ and PP strongly relate to the highly reduced actual CO,[33,34] highlighting the significant mismatch between the pump-displaced volume, that is, imposed volume rate $\dot{V}$, and the achieved hemodynamic condition.

While endoscopes are essential for imaging purposes, ensuring minimal influence on pressure and flow history is also imperative. Their presence does not affect the actual CO, yet their absence increases V_R, by 2.37 mL (35%) for BHV and 3.08 mL (35%) for PHV (Figure 5). Generally, the highest flow velocities are anticipated at the center of the orifice section,[35] and thus the absence of endoscope allows for a fully developed central jet, consequently elevating V_R during closing. Nonetheless, this pattern does not hold for the MHV, showing an 11.06 mL (45%) decrease. $\Delta\overline{P}$ increases across all valves, ranging from 0.19 to 0.78 mmHg (~2% to 19%). No obvious change on pressure history occurs, except for an elevated P_{VA} positive pressure peak during diastole for the BHV and PHV. In contrast, both minima and maxima for P_{VM} are less pronounced throughout the entire cycle across all valve types, suggesting reduced resistance (Figure 8D–F).

3.2 | Influence of hemodynamic settings

A complete valve assessment requires valve's functionality evaluation under various hemodynamic settings, and this was done with (v) and a BHV. A comparison between the P_{AO} history of hemodynamic setting ① in Figure 9 and their physiologic equivalent demonstrates close alignment. Data for $\Delta\overline{P}$, V_R, and CO for individual hemodynamic settings are available in Figure 9F. As actual CO increases, there is a corresponding rise in $\Delta\overline{P}$. A further increase can be seen for the ratio between actual CO and $\dot{V}$ as heart rate and pumping rate increase. Figure 9A presents remarkably low standard deviation, indicated by the shaded area along the curves, encompassing a mean of 10

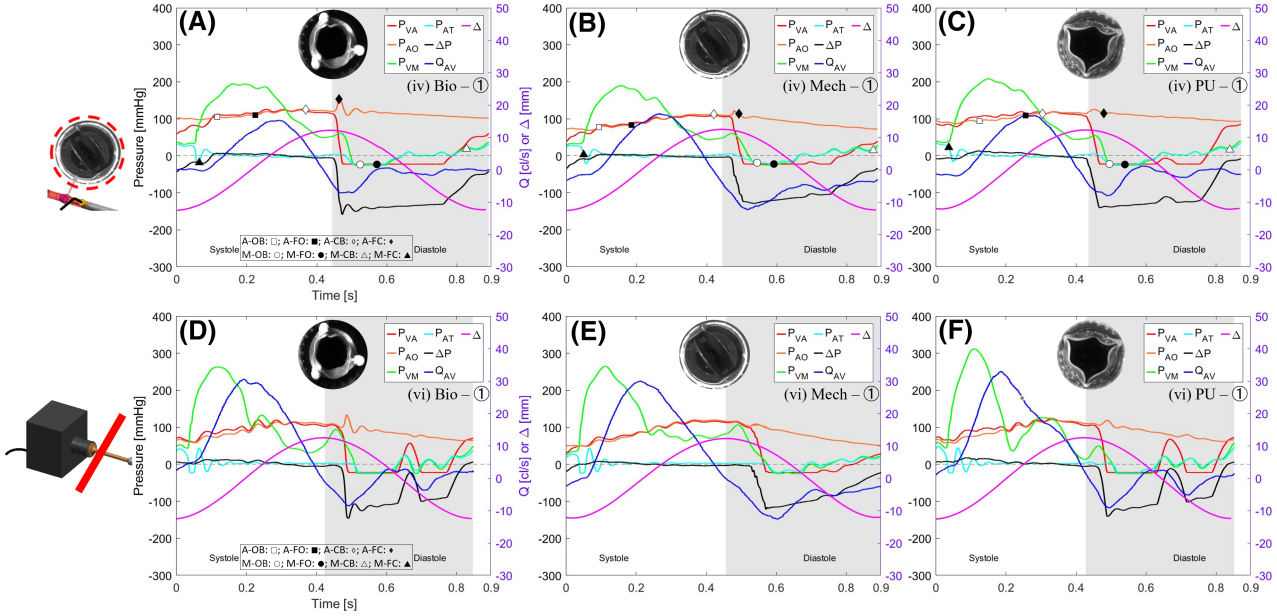

FIGURE 8 Pressure and flow history (mean of ten cycles) with alterations (iv) (A–C) and (vi) (D–F) for BHV, MHV, and PHV in aortic position with hemodynamic setting ①. A, aortic; CB, closing begins; FC, fully closed; FO, fully opened; M, mitral; OB, opening begins.

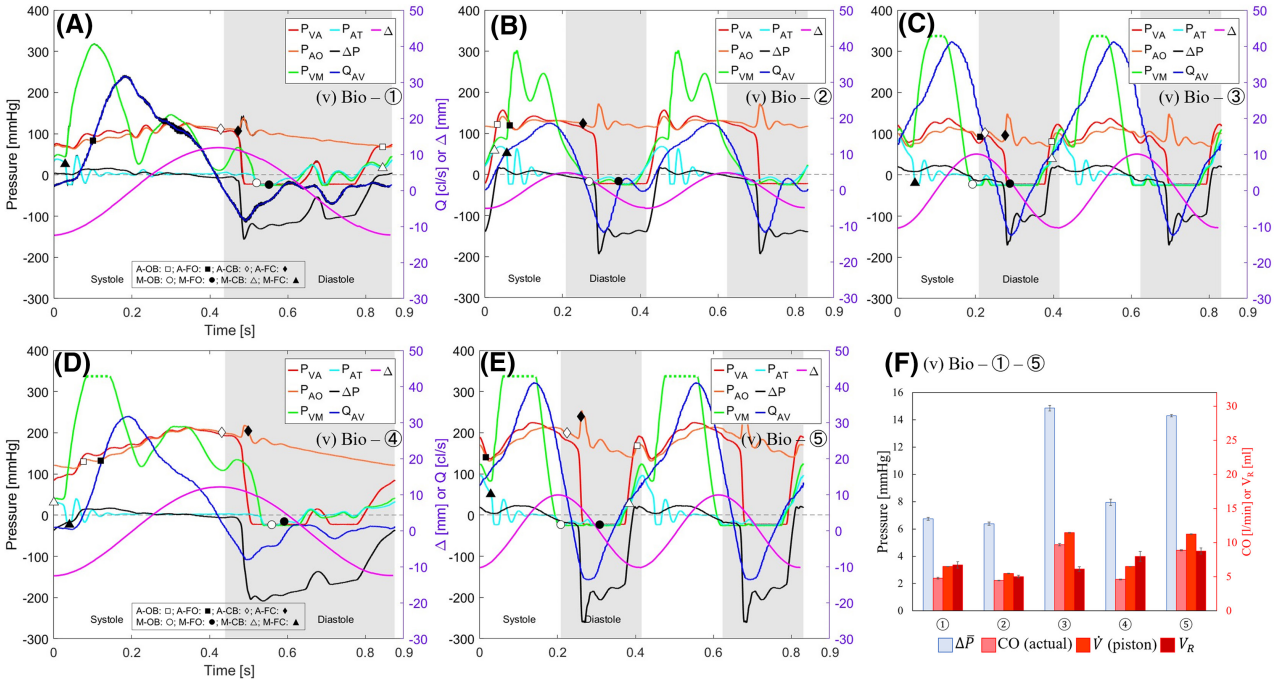

FIGURE 9 (a–e): Physiologic pressure and flow history with hemodynamic setting (A) ①, (B) ②, (C) ③, (D) ④, and (E) ⑤ and standard deviation represented as shaded area. Note that the dashed line indicates pressure beyond detection range. (F) $\Delta\overline{P}$, CO (actual), $\dot{V}$ (piston), and V_R of (v) for hemodynamic settings ① – ⑤. Similar to the MHV's effect on the aortic side (see Figure 5),

cycles, and thus PD's strong stability. Negative pressure peaks for P_{VA} during diastole are absent in healthy human individuals.[36] However, this phenomenon arises in certain piston-driven PDs, a consequence of pump's inherent high suction capability. Additionally, the elevated P_{VM} at systole's onset aligns with observations by Lanzarone et al.[6] and Durand et al.[37] They reported negative pressure at diastole onset and substantial positive pressure peaks at the beginning of systole within pump's chamber. These phenomena persist across various hemodynamic settings and most PD modifications, spanning all valve types, which is an inherent effect of piston pumps (e.g., Figures 4 and 6). For settings ③–⑤, the actual P_{VM} peak cannot be entirely displayed as the pressure exceeds sensor's acquisition range.

In fact, due to anatomical accessibility, sub-mitral ventricular pressure has not been measured to date. A CFD simulation investigating left-ventricular pressure distribution revealed that pressure directly beneath the MV surpasses that beneath the AV by ~30 mmHg,[38] while this case shows a peak-to-peak difference of 100 mmHg. The use of a rigid pulsatile pump, lacking pressure relaxation as in the human body and therefore the passive filling of the ventricle,[39] may induce negative pressure. Nevertheless, the optimized PD (v) replicates well both physiologic and pathologic AV conditions.

4 | CRITICAL REMARKS AND CONCLUSIONS

This study showed that engineered features that serve flow and pressure characteristics may equivalently lead to a reliable PD model exhibiting physiologic conditions, reducing the effort needed for high-fidelity biomimetic features. This is somewhat described in ISO 5840,[18] yet this study showed the direction on how to achieve physiologic conditions in a robust manner. For instance, rigid tubes can be combined with a compliance chamber and a flow restrictor to act as circulatory pressure resistance. Furthermore, the presence of a buffer reservoir in the atrial line proves indispensable for replicating the cardiac cycle.

Noteworthy disparities in pressure and flow history emerged across various valve prostheses. While evaluating the AV, a BHV positioned in the mitral position is favored over a mechanical counterpart, avoiding the adverse repercussions of late valve closing. Moreover, piston-based PDs may have inherent dependencies on pressure (e.g., elevated peaks or even negative ones) and flow characteristics, with respect to imposed volume and beat rate. Note also that the waveform generation capacity of the used one was confined to a systole/diastole ratio of 1/2. It is also worth mentioning that the chosen flowing medium, namely distilled water, is less viscous than blood, and this may have some minor effect on the increase of V_R (compared to blood[40]).

The most optimal of the attested PD systems is able to mimic the global framework of a native hydrodynamic environment, overlooking detailed exploration of localized fluid dynamics, biomaterial, and cellular interactions. Future investigations should delve into these aspects to provide a comprehensive understanding of valve's behavior, potential failure modes, and longevity within the physiologic context. Future studies can also explore the interaction of individual mechanical features providing further system optimization.

In summary, the thorough analysis led to a robust, versatile PD setup able to efficiently emulate both physiologic and pathologic AV hemodynamic conditions for various prosthesis types, while exposing intrinsic limitations complementing the directions proposed by the standard.

AUTHOR CONTRIBUTIONS

Caroline C. Smid was involved in conceptualization, methodology, investigation, formal analysis, software, data curation, and writing – original draft. George A. Pappas was involved in conceptualization, methodology, project administration, software, and writing – review and editing. Volkmar Falk contributed to funding acquisition and critical revision. Paolo Ermanni contributed to funding acquisition, supervision, and critical revision. Nikola Cesarovic contributed to conceptualization, methodology, supervision, and critical revision.

ACKNOWLEDGEMENTS

This work was partially funded by the ETHeart initiative from the Open ETH program by the ETH Board, and the Zurich Heart project of Hochschulmedizin Zürich. Open access funding provided by Eidgenossische Technische Hochschule Zurich.

CONFLICT OF INTEREST STATEMENT

The authors declare that they have no conflicts of interest.

ORCID

Caroline C. Smid https://orcid.org/0009-0008-2440-1892
Georgios A. Pappas https://orcid.org/0000-0003-1570-6885
Volkmar Falk https://orcid.org/0000-0002-7911-8620
Paolo Ermanni https://orcid.org/0000-0003-0158-3845
Nikola Cesarovic https://orcid.org/0000-0001-6744-2928

REFERENCES

1. Marom G, Einav S. New insights into valve hemodynamics. Rambam Maimonides Med J. 2020;11:e0014.
2. Zilla P, Brink J, Human P, Bezuidenhout D. Prosthetic heart valves: catering for the few. Biomaterials. 2008;29:385–406.
3. Butany J, Collins MJ. Analysis of prosthetic cardiac devices: a guide for the practising pathologist. J Clin Pathol. 2005;58:113–24.
4. Li KYC. Bioprosthetic heart valves: upgrading a 50-year old technology. Front Cardiovasc Med. 2019;6:47.

5. Azadani AN. In vitro experimental methods for assessment of prosthetic heart valves. Principles of heart valve engineering. Elsevier; London, UK, 2019. p. 213–38.
6. Lanzarone E, Vismara R, Fiore GB. A new pulsatile volumetric device with biomorphic valves for the in vitro study of the cardiovascular system. Artif Organs. 2009;33:1048–62.
7. Jahren SE, Heinisch PP, Wirz J, Winkler BM, Carrel T, Obrist D. Hemodynamic performance of Edwards Intuity valve in a compliant aortic root model. Annu Int Conf IEEE Eng Med Biol Soc. 2015;2015:3315–8.
8. Feng W, Yang X, Liu Y, Fan Y. An in vitro feasibility study of the influence of configurations and leaflet thickness on the hydrodynamics of deformed transcatheter aortic valve. Artif Organs. 2017;41:735–43.
9. Morisawa D, Falahatpisheh A, Avenatti E, Little SH, Kheradvar A. Intraventricular vortex interaction between transmitral flow and paravalvular leak. Sci Rep. 2018;8:15657.
10. Rodriguez RA, Dellimore KH, Müller JH. Evaluating the performance of cardiac pulse duplicators through the concept of fidelity. Cardiovasc Eng Technol. 2019;10:423–36.
11. Leo HL, Dasi LP, Carberry J, Simon HA, Yoganathan AP. Fluid dynamic assessment of three polymeric heart valves using particle image velocimetry. Ann Biomed Eng. 2006;34:936–52.
12. De Paulis R, Schmitz C, Scaffa R, Nardi P, Chiariello L, Reul H. In vitro evaluation of aortic valve prosthesis in a novel valved conduit with pseudosinuses of Valsalva. J Thorac Cardiovasc Surg. 2005;130:1016–21.
13. Singh R, Vanauker M, Joseph B, Ondrovic L, Strom JA, editors. Quantifying the effect of aortic valve degradation using signal processing techniques. 2005.
14. Adathala R, Mohan A, Charuvila M, Vayalappil MC, editors. A virtual instrumentation system for pulsatile testing of artificial heart valves. 2010.
15. Fredrick Cornhill J. An aortic-left ventricular pulse duplicator used in testing prosthetic aortic heart valves. J Thorac Cardiovasc Surg. 1977;73:550–8.
16. Duran CG, Gunning AJ, McMilian T. A simple versatile pulse duplicator. Thorax. 1964;19:503–6.
17. Vennemann B, Rösgen T, Heinisch PP, Obrist D. Leaflet kinematics of mechanical and bioprosthetic aortic valve prostheses. ASAIO J. 2018;64:651–61.
18. International Organization for Standardization 5840–3. Cardiovascular implants – Cardiac valve prostheses. 2021.
19. Wu C, Saikrishnan N, Chalekian AJ, Fraser R, Ieropoli O, Retta SM, et al. In-vitro pulsatile flow testing of prosthetic heart valves: a round-robin study by the ISO cardiac valves working group. Cardiovasc Eng Technol. 2019;10:397–422.
20. Toner G. Development of a left heart simulator for prosthetic valve evaluation. Master thesis. Drexel University; Philadelphia, Pennsylvania, 2017.
21. Bloodworth CH, Pierce EL, Easley TF, Drach A, Khalighi AH, Toma M, et al. Ex vivo methods for informing computational models of the mitral valve. Ann Biomed Eng. 2017;45:496–507.
22. Rajeev A, Mohan A, Charuvila MV, Vayalappil MC, editors. A virtual instrumentation system for pulsatile testing of artificial heart valves. 2010.
23. Jahren SE, Winkler BM, Heinisch PP, Wirz J, Carrel T, Obrist D. Aortic root stiffness affects the kinematics of bioprosthetic aortic valves. Interact Cardiovasc Thorac Surg. 2017;24:173–80.
24. Stenemo. CC BY-SA 4.0 <https://creativecommons.org/licenses/by-sa/4.0>, via Wikimedia Commons. Diagram of the human heart (no labels), https://commons.wikimedia.org/wiki/File:Diagram_of_the_human_heart_(no_labels).svg.
25. Silverthorn DU, Johnson BR, Ober WC, Ober CE, Impaglizzo A, Silverthorn AC. Human physiology: an integrated approach/Dee Unglaub Silverthorn. Global ed. Harlow: Pearson; 2019.
26. Miller-Hance WC, Gertler R. 16 – Essentials of cardiology. 6th ed. Elsevier; Philadelphia, PA, 2019.
27. Swanson M, Clark RE. Dimensions and geometric relationships of the human aortic valve as a function of pressure. Circ Res. 1974;35:871–82.
28. Leat ME, Fisher J. A synthetic leaflet heart valve with improved opening characteristics. Med Eng Phys. 1994;16:470–6.
29. Fisher J. Artificial heart valve. 1996.
30. Davis K, Muller JH, Meyer CJ, Smit FE. Evaluating the impact of air compliance chamber volumes on valve performance for three different heart valves. 2018 3rd biennial south African biomedical engineering conference (SAIBMEC). Stellenbosch, IEEE 2018, p. 1–4.
31. O'Rourke MF, Hashimoto J. Mechanical factors in arterial aging: a clinical perspective. J Am Coll Cardiol. 2007;50:1–13.
32. Carrel T, Dembitsky WP, de Mol B, Obrist D, Dreyfus G, Meuris B, et al. Non-physiologic closing of bi-leaflet mechanical heart prostheses requires a new tri-leaflet valve design. Int J Cardiol. 2020;304:125–7.
33. Saugel B, Kouz K, Scheeren TWL, Greiwe G, Hoppe P, Romagnoli S, et al. Cardiac output estimation using pulse wave analysis-physiology, algorithms, and technologies: a narrative review. Br J Anaesth. 2021;126:67–76.
34. Marquez J, McCurry K, Severyn DA, Pinsky MR. Ability of pulse power, esophageal doppler, and arterial pulse pressure to estimate rapid changes in stroke volume in humans. Crit Care Med. 2008;36:3001–7.
35. Tango AM, Salmonsmith J, Ducci A, Burriesci G. Validation and extension of a fluid-structure interaction model of the healthy aortic valve. Cardiovasc Eng Technol. 2018;9:739–51.
36. Sabbah HN, Anbe DT, Stein PD. Negative intraventricular diastolic pressure in patients with mitral stenosis: Evidence of left ventricular diastolic suction. The American Journal of Cardiology 1980;45:562–66.
37. Durand LG, Garcia D, Sakr F, Sava H, Cimon R, Pibarot P. A new flow model for Doppler ultrasound study of prosthetic heart valves. J Heart Valve Dis 1999; 8:85–95.
38. Ahmad Bakir A, Al Abed A, Stevens MC, Lovell NH, Dokos S. A Multiphysics Biventricular Cardiac Model: Simulations With a Left-Ventricular Assist Device. Front Physiol 2018; 9:1259.
39. Choi HF, D'hooge J, Rademakers FE, Claus P. Influence of left-ventricular shape on passive filling properties and end-diastolic fiber stress and strain. J Biomech 2010;43:1745–53.
40. Pohl M, Wendt MO, Werner S, Koch B, Lerche D. In vitro testing of artificial heart valves: comparison between Newtonian and non-Newtonian fluids. Artif Organs 1996;20:37–46.

How to cite this article: Smid CC, Pappas GA, Falk V, Ermanni P, Cesarovic N. A parametric study on pulse duplicator design and valve hemodynamics. Artif. Organs. 2024;00:1–11. https://doi.org/10.1111/aor.14757